

Article

# Exploring the Impact of Palladium Loading on Pd-Based Three-Way Catalyst Performance and Propane Reactivity for Emission Reduction in Liquefied Petroleum Gas Engines

Daekun Kim <sup>†</sup> 

Department of Mechanical, Aerospace, and Biomedical Engineering, University of Tennessee, Knoxville, TN 37996, USA; magic15123@gmail.com

<sup>†</sup> Current address: Department of Civil, Environmental, and Construction Engineering, University of Central Florida, Orlando, FL 32816, USA.

**Abstract:** To reduce air pollution worldwide, regulations on exhaust gas emissions from ships are becoming increasingly stringent. One fuel that is being considered as an alternative to replace the heavy fuel oil used in existing ship engines and thereby reduce harmful emissions, such as NO<sub>x</sub>, SO<sub>x</sub>, and greenhouse gases, is sulfur-free liquefied petroleum gas (LPG). To assess the viability of this alternative, it is necessary to understand propane reactivity, the main component of LPG, and develop after-treatment devices applicable to LPG engines. This research evaluated the performance of three prototype Pd-based three-way catalysts (TWCs) with varying Pd loadings (6.5, 4.1, and 1.4 g/L), focusing on their effectiveness concerning propane reactivity in LPG engines. For the fresh samples, catalysts with 4.1 g/L Pd demonstrated performance that was comparable to, or even surpassed, those containing 6.5 g/L Pd. Notably, the temperature of 50% conversion (T<sub>50</sub>) for NO and C<sub>3</sub>H<sub>8</sub> in the fresh Pd-4.1 was lower by 14 °C and 10 °C, respectively, compared to the fresh Pd-6.5 sample, despite having 37% less precious-metal loading. However, after hydrothermal aging at 900 °C for 100 h, the performance of the 4.1 g/L Pd catalyst significantly deteriorated, exhibiting lower efficiency than the 6.5 g/L Pd catalyst. The study also delved into various probe reactions, including the water–gas shift and propane steam reforming. Advanced analytical techniques, such as N<sub>2</sub> physisorption and scanning transmission electron microscopy, were employed to elucidate the texture and structural characteristics of the catalyst, providing a comprehensive understanding of its behavior and potential applications. Through this research, within the efforts of the maritime sector to address challenges posed by emission regulations and rising costs associated with precious metals, this study has the potential to contribute to the development of cost-effective emission control solutions.

**Keywords:** Pd-based three-way catalyst; ceria-zirconia mixed oxide; liquefied petroleum gas; propane engine; water–gas shift reaction; steam-reforming reaction



**Citation:** Kim, D. Exploring the Impact of Palladium Loading on Pd-Based Three-Way Catalyst Performance and Propane Reactivity for Emission Reduction in Liquefied Petroleum Gas Engines. *J. Mar. Sci. Eng.* **2023**, *11*, 2187. <https://doi.org/10.3390/jmse11112187>

Academic Editor: Peter Vidmar

Received: 24 October 2023

Revised: 12 November 2023

Accepted: 14 November 2023

Published: 17 November 2023



**Copyright:** © 2023 by the author. Licensee MDPI, Basel, Switzerland. This article is an open access article distributed under the terms and conditions of the Creative Commons Attribution (CC BY) license (<https://creativecommons.org/licenses/by/4.0/>).

## 1. Introduction

For decades, global efforts have been made to reduce emissions from vehicles that contribute significantly to global warming and have harmful effects on human health. In line with this, maritime emissions have come under increased scrutiny, leading to stricter regulations on exhaust gases from ships [1]. To reduce sulfur oxides (SO<sub>x</sub>) emissions, the International Maritime Organization (IMO) has limited the sulfur (S) content in the heavy fuel oil used as ship fuel from 3.5% to 0.5% through the International Convention for the Prevention of Pollution from Ships (MARPOL) Annex 6, which took effect on 1 January 2020 [2,3]. Since 2016, nitrogen oxides (NO<sub>x</sub>) emissions from marine diesel engines have had to meet IMO Tier III regulations in designated Emission Control Areas (ECAs), and since that time, the IMO Tier III regulations have extended to other regions [2]. To comply with these restrictions, ships that are currently being built are attempting to eliminate NO<sub>x</sub> by applying after-treatment systems such as selective catalytic reduction (SCR) [4,5]

or exhaust gas recirculation (EGR) [6,7]. However, recent studies have shown that the capacity of SCR catalysts to significantly improve NO<sub>x</sub> reduction ability is limited because of the degradation of catalyst performance due to sulfur poisoning. Additional research on catalyst life is needed in the future [8].

The shipping industry contributes to 3% of the global annual greenhouse gas (GHG) emissions [9], predominantly deriving its energy for vessel propulsion from fossil fuels. In this context, there is a growing interest in the use of eco-friendly fuels to reduce harmful emissions, such as NO<sub>x</sub>, SO<sub>x</sub>, and particulate matter (PM) emitted from marine diesel engines. Alternative fuels that do not contain S, such as liquefied natural gas (LNG), biodiesel, and liquefied petroleum gas (LPG), are currently being considered as alternatives [10]. According to recent studies, dual-fuel engines using LNG [11,12] and LPG [13–15] emit fewer toxic emissions such as CO, PM, SO<sub>x</sub>, and NO<sub>x</sub> than conventional diesel engines. In particular, LPG, with its low carbon content and straightforward molecular structure, has the added advantage of reducing post-combustion fine dust [16]. An analysis of greenhouse gas (GHG) and reference pollutant emissions has shown that the carbon content of LPG is lower than that of conventional gasoline and diesel fuel, reducing GHG emissions [17,18]. Given these benefits, the development of marine engines compatible with LPG is underway. However, propane (C<sub>3</sub>H<sub>8</sub>), which is the main component of LPG, has relatively slow reactivity due to its stable chemical structure in comparison with other HCs such as C<sub>3</sub>H<sub>6</sub>, C<sub>7</sub>H<sub>8</sub>, C<sub>8</sub>H<sub>10</sub>, and C<sub>8</sub>H<sub>18</sub> [19,20]. Simultaneously, there is a pressing requirement to engineer catalysts for these engines that can efficiently mitigate emissions, particularly during cold start conditions. Recent research has focused on applying three-way catalysts (TWCs) to heavy-duty engines using alternative fuels [21]. While there have been modeling efforts to understand TWC mechanisms [22,23], most of these studies have centered around natural gas in heavy-duty engines. Therefore, it is important to investigate propane as a sole unburned hydrocarbon (UHC) in this context, addressing a critical research gap and using LPG as an alternative fuel.

The TWC, which has been widely used as an after-treatment device for conventional gasoline engines, may be considered for application to marine gas fuel engines to meet IMO Tier III NO<sub>x</sub> emission standards. Commonly, TWCs containing precious metals have been widely employed to reduce CO, NO<sub>x</sub>, and HCs emitted from gasoline engines through oxidation and reduction reactions [24]. TWCs often incorporate promoters like CeO<sub>2</sub> and ZrO<sub>2</sub> to enhance performance and stave off deactivation [25–27]. The oxygen storage material, mixed oxides (Ce-Zr) is coated on the monolith to serve as an oxygen buffer and to improve thermal durability. The active metals most often used in TWCs are Pd, Pt, and Rh, with γ-Al<sub>2</sub>O<sub>3</sub> as a support for high surface areas. Among these precious metals, Pd has been widely used as a precious metal for TWCs due to its ability to reduce hydrocarbons and its superior resistance to thermal aging [28,29]. However, with the escalating costs of precious metals, there is a pressing economic imperative to optimize their loading in TWCs. The challenge lies in achieving a delicate balance: reducing the precious-metal content to ensure cost-effectiveness while ensuring that the catalyst's performance remains uncompromised.

In the face of emerging challenges in the maritime sector and the growing emphasis on eco-friendly alternatives, an evaluation was conducted on prototype Pd-based TWCs with different Pd loadings (6.5, 4.06, and 1.41 g/L) using a bench-flow reactor (BFR), specifically targeting their efficacy in propane reactivity within LPG engines. Through temperature ramping experiments, the reactivity of C<sub>3</sub>H<sub>8</sub> within these catalysts was meticulously investigated under stoichiometric conditions. Furthermore, insights into the catalyst's capabilities were broadened by investigating oxygen storage capacity (OSC) and various probe reactions, including the water–gas shift (WGS) and propane steam reforming (SR). Advanced analytical techniques, such as N<sub>2</sub> physisorption and STEM, were employed to elucidate the texture and structural characteristics of the catalyst. Drawing upon the investigated results, this research endeavors to provide a foundation for the maritime

industry to move toward more efficient and economical emission control solutions, with a particular focus on optimizing the use of precious metals in TWCs.

## 2. Materials and Methods

### 2.1. Bench Flow Reactor (BFR) System

Figure 1 presents a schematic diagram of the bench flow reactor (BFR). The simulated exhaust gas was introduced into a TWC reactor from high-pressure gas cylinders using mass flow controllers (MFCs). Water flowed into the BFR system in a vapor state through a steam generator with  $N_2$  gas. The TWC reactor consisted of a quartz tube with an external diameter of 25 mm and a length of 43 cm, which was placed inside a Lindberg Mini-Mite furnace. The upstream portion of the quartz tube was filled with quartz beads 5 mm in diameter, heating the inlet gas uniformly and introducing well-mixed simulated gas into the TWC. TWC samples with a diameter of 2.2 cm and a length of 2.54 cm were wrapped in ULTRA-TEMP 390 ceramic tape and placed in the downstream section of the quartz tube close to the furnace exit. Three Omega type-K thermocouples were used to measure the inlet and outlet temperatures of the simulated gas and the temperature of the catalyst surface. Two thermocouples located opposite the TWC, approximately 5 mm from the entrance and exit, were used to measure the inlet gas temperature and TWC exit gas temperature. The remaining thermocouple inside the TWC was used to measure the temperature in the middle of the catalyst. A MIDAC Fourier transform infrared analyzer (FTIR) was used to measure NO, CO,  $C_3H_8$ ,  $NH_3$ ,  $N_2O$  and  $CO_2$  concentrations.

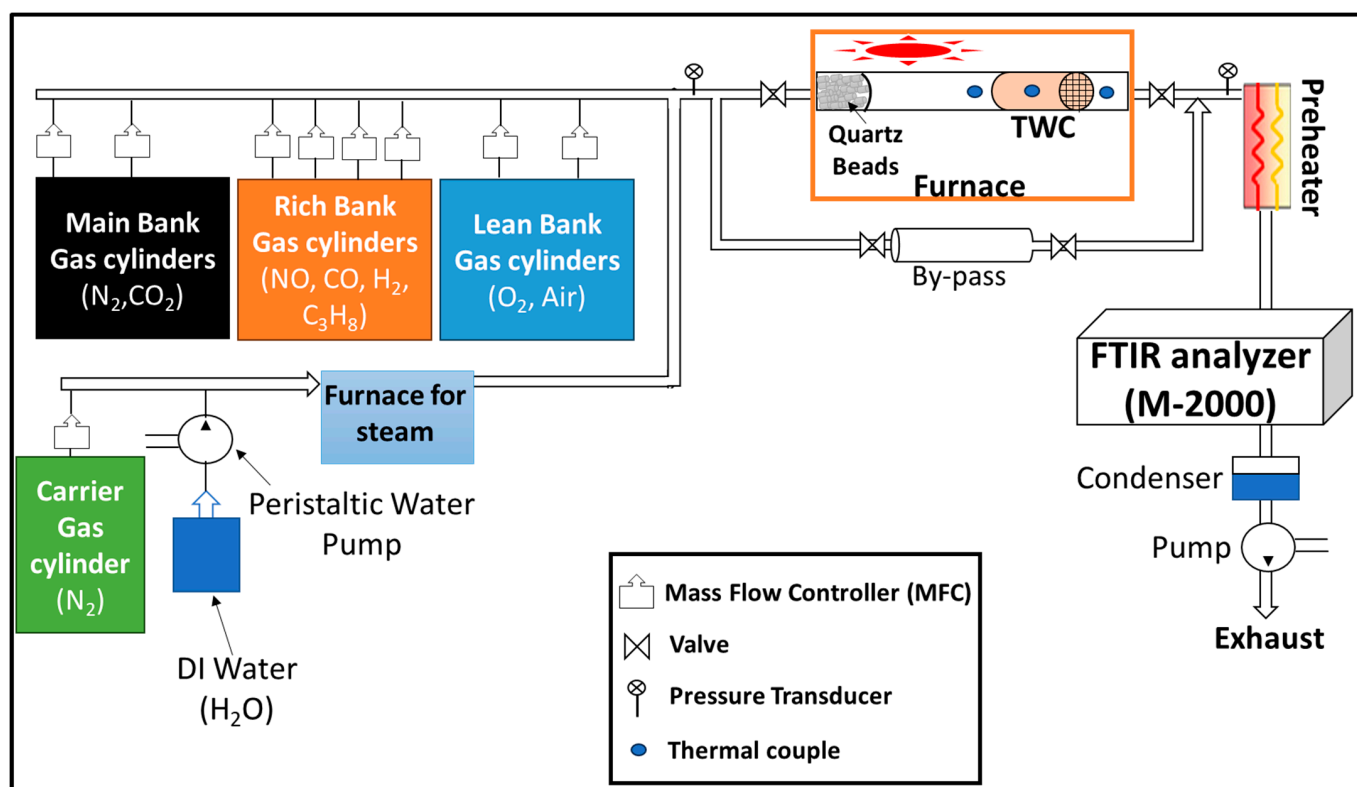


**Figure 1.** Schematic diagram of the bench flow reactor (BFR) system.

### 2.2. Three-Way Catalysts (TWCs) and Hydrothermal Aging Protocol

In this study, Pd was the only precious metal included in the TWC samples. To investigate the effect of Pd loading on  $C_3H_8$  reactivity, three different formulations of a family of prototype TWCs were prepared. While each TWC sample contained mixed oxides (Ce-Zr) serving as the OSC material, they varied in Pd loading, as detailed in Table 1. Since

the TWC samples prepared for this study were prototypes, the exact composition of the catalyst cannot be identified.

**Table 1.** Characteristics of PGM loading and OSC material in different samples.

Sample	Pd Loading (g/L)	OSC Material
Pd-6.5	6.50	Present
Pd-4.1	4.06	Present
Pd-1.4	1.41	Present

The TWC samples underwent a hydrothermal aging (HTA) process in a furnace maintained at 900 °C for a span of 100 h, adhering to the protocols established by the Cross-Cut Lean Exhaust Emission Reduction Simulations (CLEERS) specifically designed for gasoline engines [30]. The procedure began in a neutral setting, comprising 10% CO<sub>2</sub>, 10% H<sub>2</sub>O, and the rest being N<sub>2</sub>, lasting for 40 s. This stage was succeeded by a 10 s period in rich conditions, marked by 10% CO<sub>2</sub>, 10% H<sub>2</sub>O, 3% CO, and 1% H<sub>2</sub>, with the remaining as N<sub>2</sub>. The cycle concluded with an additional 10 s in lean conditions, featuring 10% CO<sub>2</sub>, 10% H<sub>2</sub>O, 3% O<sub>2</sub>, and the rest as N<sub>2</sub>. It is worth noting that due to the poor performance of the Pd-4.1 TWC sample, the HTA process was not carried out.

### 2.3. Bench Flow Evaluation Protocols

To stabilize all fresh TWC samples, a de-greening process was conducted on the BFR. The gas composition consisted of 10% of CO<sub>2</sub>, 10% of H<sub>2</sub>O, and balanced N<sub>2</sub>, and the process was conducted at an inlet gas temperature of 700 °C for 4 h at GHSV 60,000 h<sup>-1</sup>. The temperature sweep experiment increased the furnace temperature from 100 °C to 600 °C by 5 °C per min to obtain light-off curves of C<sub>3</sub>H<sub>8</sub> and NO as a function of the inlet gas temperatures. The simulated exhaust gases consisted of 0.3% C<sub>3</sub>H<sub>8</sub>, 0.5% CO, 0.1% NO, 0.167% H<sub>2</sub>, 0.78% O<sub>2</sub>, 13% H<sub>2</sub>O, 13% CO<sub>2</sub>, and balanced N<sub>2</sub>. The conversion of NO, CO, and C<sub>3</sub>H<sub>8</sub> was calculated by Equation (1).

$$X_{\text{gas}} = \frac{G_{\text{as in}} - G_{\text{as out}}}{G_{\text{as in}}} \times 100\% \quad (1)$$

where  $X_{\text{gas}}$  is the conversion of gas (%) and  $G_{\text{as in}}$  and  $G_{\text{as out}}$  are the concentration of each gas (NO, CO, and C<sub>3</sub>H<sub>8</sub>) at the inlet and outlet of the reactor (ppm), respectively.

The effectiveness of the WGS and SR reactions, which act as indicative reactions for the TWC, was analyzed to gauge the influence of the OSC material. Both reactions were tested under comparable temperature settings. The temperature was methodically raised from 200 °C to 550 °C at 5 °C per min increments. For the WGS reaction, a gas combination of 0.5% CO and 13% H<sub>2</sub>O, balanced with N<sub>2</sub>, was employed. On the other hand, the SR reaction was conducted using a gas blend of 0.1% C<sub>3</sub>H<sub>8</sub>, and 13% H<sub>2</sub>O, with the remainder being N<sub>2</sub>.

The supplied gas composition and duration during the lean and rich cycles are listed in Table 2. The oxygen storage capacity (OSC) of the fresh TWC samples was measured at an inlet gas temperature of 350 and 550 °C using a slow cycle consisting of 20 min lean and 5 min rich for a total of three cycles. The OSC was calculated based on the amount of CO<sub>2</sub> generated during the fuel-rich cycle, as determined by Equation (2).

$$\text{OSC} = \frac{\int_{t_0}^t (Y_{\text{CO}_2}) dt}{L_{\text{Cat}}} \times 32 \quad (2)$$

where OSC is the oxygen storage capacity (g/L),  $Y_{\text{CO}_2}$  is the formation of CO<sub>2</sub> (mol),  $L_{\text{cat}}$  is the volume of catalyst (l), and the value of 32 is the molar mass of O<sub>2</sub> (g/mol), which is to convert moles of CO<sub>2</sub> into grams.

**Table 2.** Gas compositions for OSC measurements.

Mode	Time (min)	Gas Composition
Lean	20	1.5% O <sub>2</sub> and balance N <sub>2</sub>
Rich	5	0.2% CO and balance N <sub>2</sub>

#### 2.4. Surface Characterization Studies

N<sub>2</sub> physisorption tests were conducted on a Quantachrome gas sorption apparatus (Autosorb iQ) to analyze the pore configuration and surface area of the catalyst samples. Before the analysis, the samples were degassed at 300 °C for a duration of 4 h. The Brunauer–Emmett–Teller (BET) technique was employed to determine the surface area, and the Barrett–Joyner–Halenda (BJH) approach was utilized to measure pore volume and pore size distribution. BET surface area was calculated by Equation (3).

$$S_{BET} = \frac{S_{total}}{w} \quad (3)$$

where  $S_{BET}$  is specific surface area BET (m<sup>2</sup>/g),  $S_{total}$  is total surface area (m<sup>2</sup>), and  $w$  is the weight of the solid sample (g).

The imaging and analysis of the samples were carried out using an FEI Talos F200X TEM/STEM, operating at an accelerating voltage of 200 kV. This equipment provided detailed microstructural observations and elemental evaluations, with a focus on assessing Pd distribution and measuring particle size, notably after undergoing hydrothermal aging.

### 3. Results and Discussion

#### 3.1. Texture of Catalysts

Table 3 presents the surface properties (surface area, pore volume, and average pore size) of the fresh and hydrothermal-aged (HTA) TWC samples using N<sub>2</sub> physisorption. The Pd-6.5 and Pd-4.1 samples showcased closely aligned specific surface areas, falling between 41.7 m<sup>2</sup>/g and 42.5 m<sup>2</sup>/g. This similarity in surface area, despite different Pd loadings, suggests that the initial dispersion and distribution of Pd on the support were relatively consistent between these samples. Both samples had an identical average pore size of 12.6 nm, further reinforcing the notion of their structural similarity at the onset. However, the Pd-4.1 sample distinguished itself with the highest pore volume. This elevated pore volume could be indicative of a more porous structure or the presence of larger mesopores, which might influence reactant accessibility and diffusion within the catalyst. The Pd-1.4 sample deviated significantly in its surface properties, underscoring the potential impact of its reduced Pd loading on its structural and morphological attributes. In the hydrothermal-aged TWC samples, both the Pd-6.5 and Pd-4.1 samples saw their surface areas and pore volumes diminish, while their pore sizes expanded. This increase in pore size, coupled with the reduction in surface area, is a classic indication of sintering or pore coalescence. Such structural alterations can be attributed to the high-temperature aging process, which can induce particle migration and growth, leading to the agglomeration of active sites and the merging of adjacent pores. Consistent with the trend observed in the fresh samples, the Pd-4.1 sample maintained a larger pore size than the Pd-6.5 sample even after hydrothermal aging. In heterogeneous catalysis, the dispersion and distribution of the active metal phase, in this case, Pd, can slightly impact the overall porous structure of the catalyst. Higher Pd loadings, as seen in the Pd-6.5 sample, might lead to larger Pd clusters or particles, potentially occupying or blocking some of the pores, thereby reducing the available pore volume. Conversely, a sample with a slightly reduced Pd loading, like Pd-4.1, might have smaller, more uniformly dispersed Pd particles, preserving the inherent porous structure of the support material and resulting in a larger pore volume. Furthermore, the interaction between Pd and the support can also play a pivotal role. Different Pd loadings might alter the strength and nature of these interactions, potentially influencing the stability and

resistance of the porous structure to sintering and other degradative effects, especially during hydrothermal aging.

**Table 3.** BET surface areas ( $S_{\text{BET}}$ ), pore volumes, and average pore sizes of fresh and hydrothermal-aged TWC samples.

Sample		$S_{\text{BET}}$ ( $\text{m}^2/\text{g}$ )	Pore Volume * ( $\text{cm}^3/\text{g}$ )	Average Pore Size * (nm)
Pd-6.5	Fresh	42.5	0.23	12.6
	HTA	21.2	0.19	17.8
Pd-4.1	Fresh	41.7	0.26	12.6
	HTA	23.6	0.22	17.7
Pd-1.4	Fresh	30.4	0.23	18.0
	HTA	-	-	-

\* Determined using Barrett–Joyner–Halenda (BJH) method. Note: Hydrothermal aging for the Pd-1.4 sample was not conducted due to its poor performance.

### 3.2. Bench-Flow Reactor (BFR) Performance Assessment

#### 3.2.1. Performance of TWCs

Figure 2 illustrates the light-off curves related to the conversion of NO, CO, and  $\text{C}_3\text{H}_8$  for the fresh TWC samples Pd-6.5, Pd-4.1, and Pd-1.4, as well as the hydrothermally aged TWC samples Pd-6.5 and Pd-4.1. Also, these curves depict the production of  $\text{NH}_3$  and  $\text{N}_2\text{O}$ . Subsequently, Figure 3 represents the temperature of 50% conversion ( $T_{50}$ ) and 90% conversion ( $T_{90}$ ) values obtained from the light-off curves for the conversion of NO, CO, and  $\text{C}_3\text{H}_8$ . Upon a detailed examination of the TWC performance for propane engine exhaust-gas conversion based on Pd loading in fresh samples, both the Pd-6.5 and Pd-4.1 samples exhibited similar CO conversion performances. However, despite having a lower Pd loading, the Pd-4.1 sample outperformed the Pd-6.5 sample in terms of NO and  $\text{C}_3\text{H}_8$  conversion. In particular, the NO conversion of the Pd-6.5 sample was observed to be lower than that of the Pd-4.1 sample at temperatures exceeding 300 °C, and its  $T_{50}$  for NO conversion was 14 °C higher than the Pd-4.1 sample. This observation suggests that increased Pd concentrations might not linearly enhance  $\text{C}_3\text{H}_8$  conversion efficiency. Additionally, the Pd-4.1 sample showed heightened  $\text{NH}_3$  production at these elevated temperatures. This suggests that  $\text{H}_2$ , potentially derived from the water–gas shift (WGS) reaction or steam-reforming (SR) reaction on Pd sites and OSC components, could serve as a more potent reducing agent for NO in the Pd-4.1 sample [31,32]. The Pd-1.4 sample, with a reduced Pd loading of 1.4 g/L, showed significantly lower TWC performance.

On the other hand, upon examining the hydrothermally aged TWC samples, it was evident that the conversion performance of TWC in the Pd-4.1 sample was more adversely impacted by hydrothermal aging at 900 °C compared to the Pd-6.5 sample. Specifically, the  $T_{50}$  values for NO, CO, and  $\text{C}_3\text{H}_8$  in the Pd-4.1 sample were higher by 76 °C, 3 °C, and 19 °C, respectively, when compared to the Pd-6.5 sample. Similarly, the  $T_{90}$  values for these gases in the Pd-4.1 sample were elevated by 94 °C, 9 °C, and 71 °C, respectively. In the fresh samples, both the Pd-4.1 and Pd-6.5 samples exhibited similar performance due to the well-dispersed nature of Pd. However, after hydrothermal aging, the performance disparity between the two samples became more pronounced. This divergence can be attributed to the sintering of Pd, which leads to the agglomeration of Pd particles, reducing their active surface area and consequently diminishing their catalytic activity. While the Pd-4.1 sample, with its 37% reduced Pd loading, presents an economically attractive option, the challenges introduced by Pd sintering underscore the importance of ensuring catalyst durability, especially when faced with hydrothermal aging.

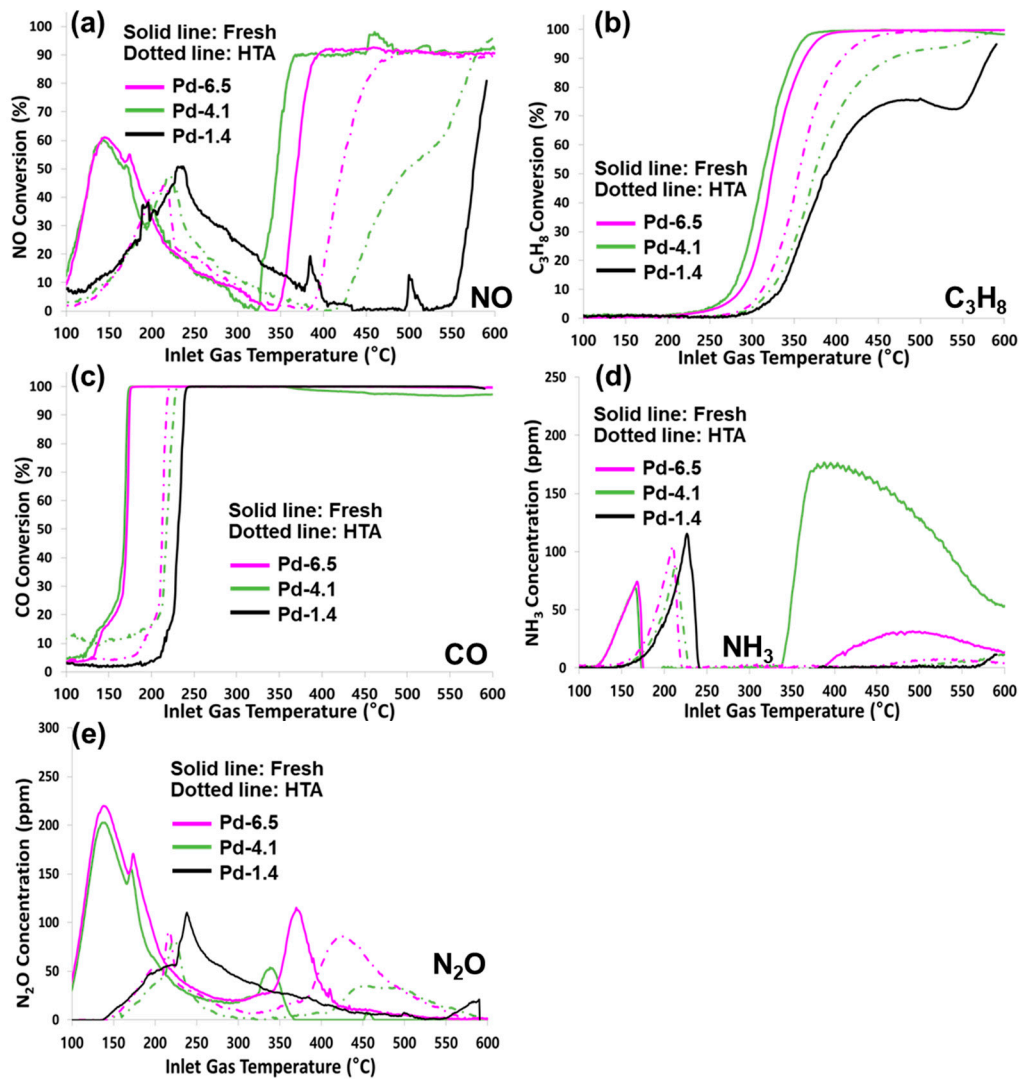


Figure 2. Effect of inlet gas temperature on the conversion of (a) NO, (b) C<sub>3</sub>H<sub>8</sub>, and (c) CO and the formation of (d) NH<sub>3</sub> and (e) N<sub>2</sub>O for fresh Pd-6.5, Pd-4.1, and Pd-1.4 and for HTA Pd-6.5 and Pd-4.1 samples in a stoichiometric condition.

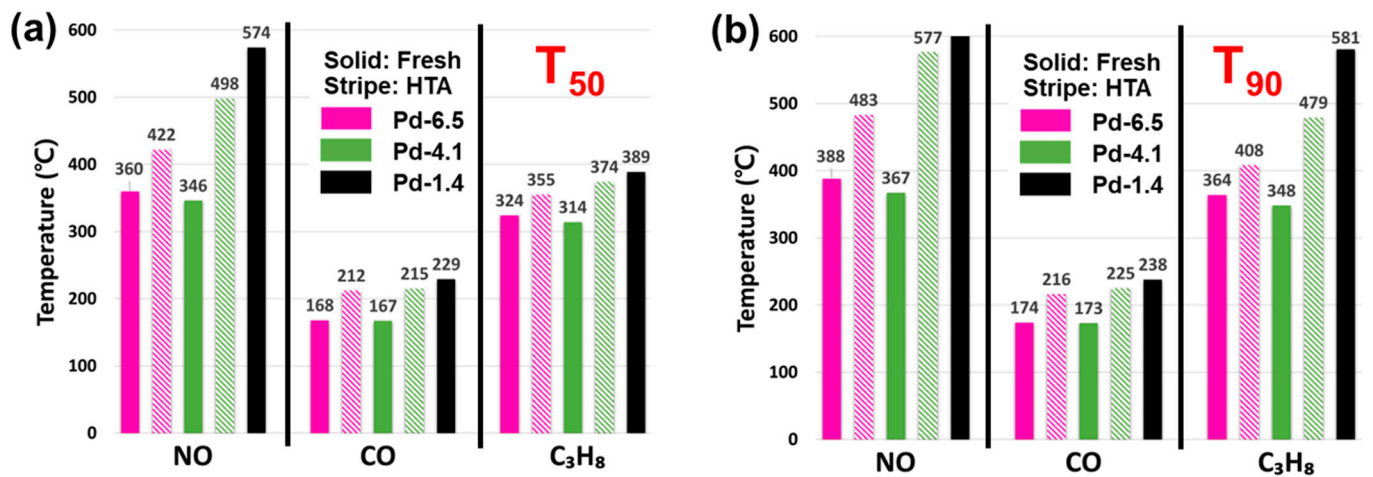
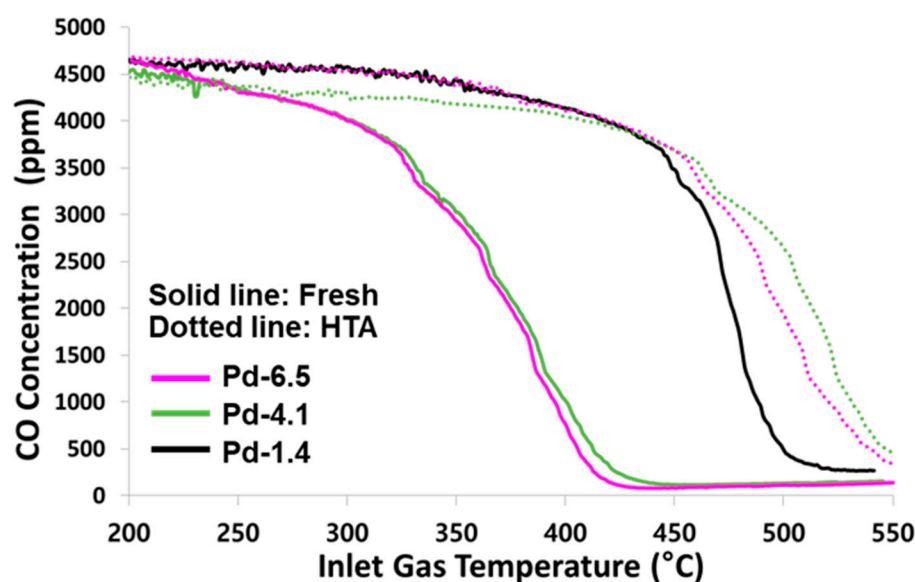


Figure 3. (a) T<sub>50</sub> and (b) T<sub>90</sub> of NO, CO, and C<sub>3</sub>H<sub>8</sub> for fresh Pd-6.5, Pd-4.1, and Pd-1.4 and for HTA Pd-6.5 and Pd-4.1 samples in a stoichiometric condition.

### 3.2.2. Probe Reactions and Oxygen Storage Capacity

In our comprehensive analysis of the water–gas shift (WGS) and propane steam-reforming reactions, as illustrated in Figures 4 and 5, respectively, we observed variations influenced by Pd loading and hydrothermal aging. Figure 4 illustrates that the WGS performance of fresh Pd-6.5 and Pd-4.1 samples was remarkably similar. This suggests that factors beyond Pd loading, such as OSC performance, play a role [33]. This consistency suggests that within the studied Pd loading range, the catalysts exhibit a uniform proficiency in facilitating the WGS reaction. The comparable efficiency between Pd-6.5 and Pd-4.1 samples further implies a consistent distribution of catalytic activity. Conversely, the Pd-1.4 sample, characterized by its lower Pd loading, displayed notably diminished performance, hinting at a potential Pd concentration threshold below which efficiency significantly diminishes. Upon hydrothermal aging at 900 °C, the WGS performance of the Pd-6.5 sample marginally surpassed that of the Pd-4.1 sample. This subtle advantage suggests that the Pd-6.5 sample's higher Pd loading might confer slight benefits in the WGS reaction. Nevertheless, both samples manifested analogous degradation trends, indicating a shared susceptibility to hydrothermal aging within the 4.1 to 6.5 Pd loading range.



**Figure 4.** Conversion of CO in water–gas shift (WGS) reaction for fresh Pd-6.5, Pd-4.1, and Pd-1.4, and HTA samples for Pd-6.5 and Pd-4.1 samples.

In our examination of the propane steam-reforming (SR) reaction, depicted in Figure 5, distinct performance differences were evident among the Pd-6.5, Pd-4.1, and Pd-1.4 TWC samples. The Pd-6.5 sample, characterized by its higher Pd loading, consistently outperformed the Pd-4.1 sample in the SR reaction. In line with its WGS reaction trend, the Pd-1.4 sample exhibited the poorest performance in the SR reaction. When subjected to hydrothermal aging at 900 °C, both samples showed signs of performance degradation, underscoring their shared vulnerability to such conditions. However, the Pd-6.5 sample maintained a relatively stronger performance, emphasizing its enhanced catalytic efficiency in the SR reaction.

Figure 6 presents the oxygen storage capacity (OSC) results of the tested TWC samples at 350 and 550 °C. At 350 °C, the fresh Pd-6.5 and Pd-4.1 samples displayed similar OSC values, suggesting that at this temperature, the OSC performance is relatively consistent between these samples. However, at 550 °C, a divergence in performance was observed. The Pd-4.1 sample exhibited an OSC value of 2.77 g/Lcat, surpassing the 2.24 g/Lcat of the Pd-6.5 sample. This heightened OSC in the Pd-4.1 sample can potentially be attributed to its larger pore volume, as referenced in Table 3. This increased pore volume might enhance oxygen storage and release dynamics, leading to improved OSC performance [33,34].

In contrast, the Pd-1.4 sample, characterized by its lower Pd content, demonstrated a markedly reduced OSC across both temperatures, emphasizing the significance of Pd loading in influencing OSC performance.

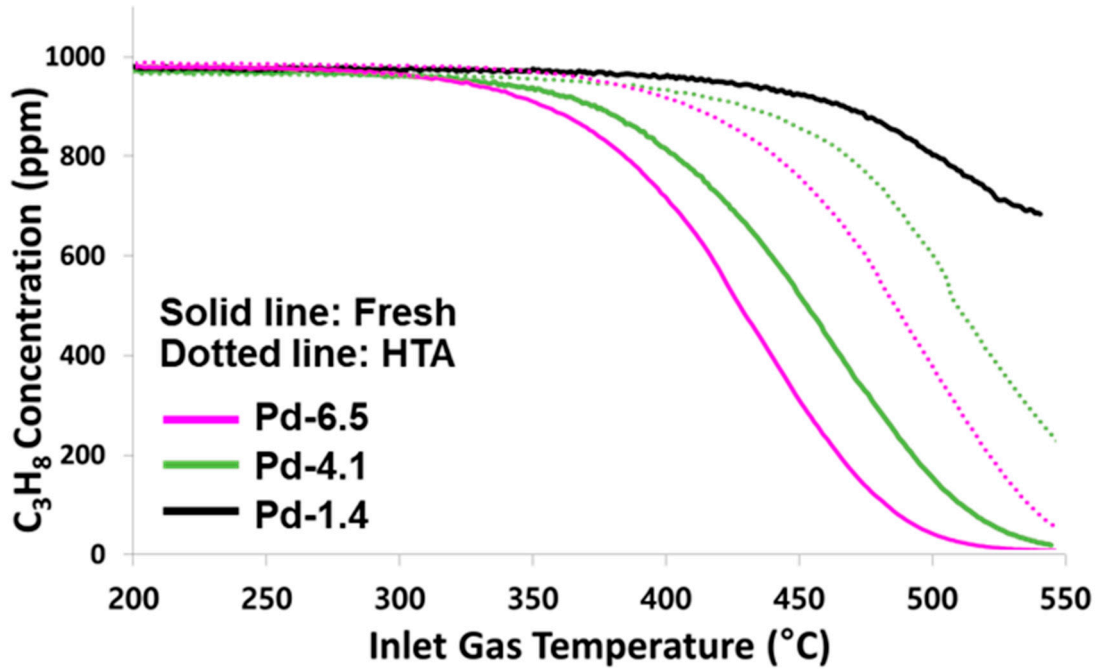


Figure 5. Conversion of C<sub>3</sub>H<sub>8</sub> in steam-reforming (SR) reaction for fresh Pd-6.5, Pd-4.1, and Pd-1.4, and HTA samples for Pd-6.5 and Pd-4.1 samples.

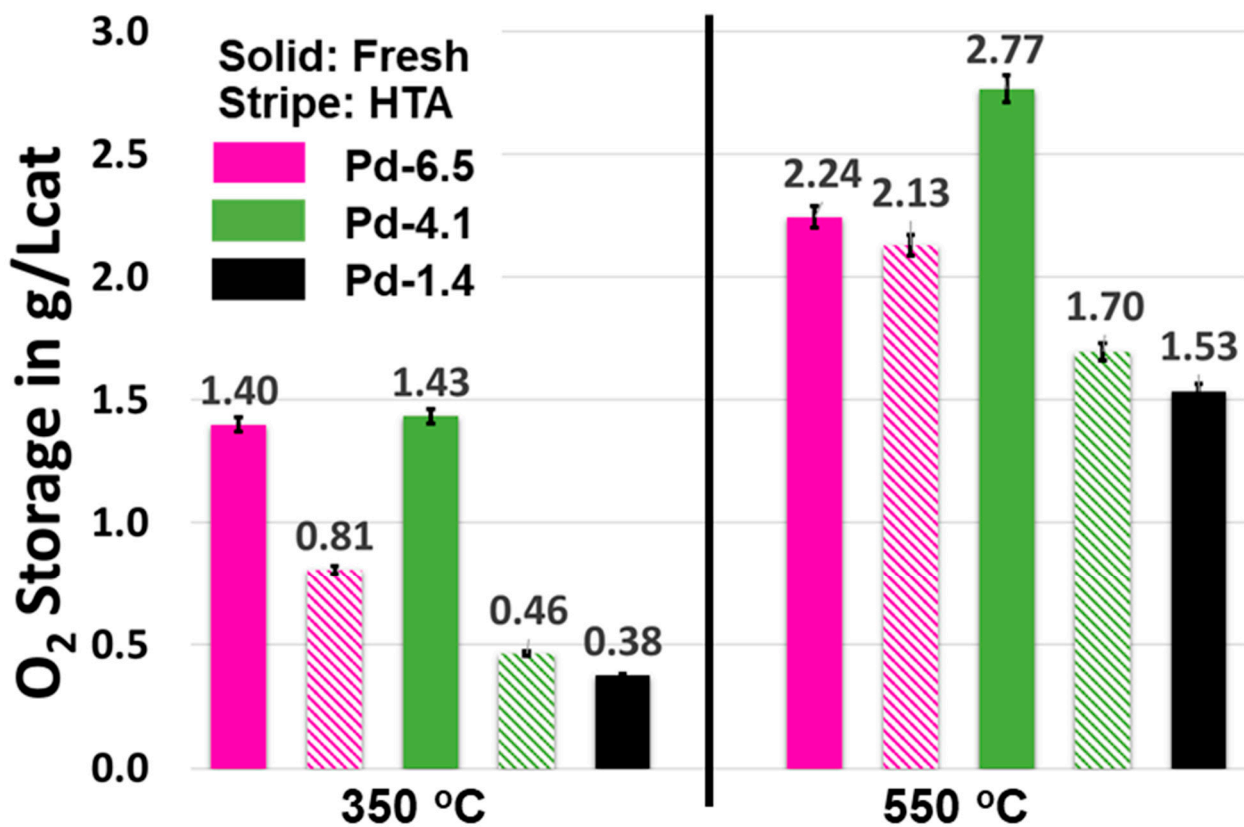
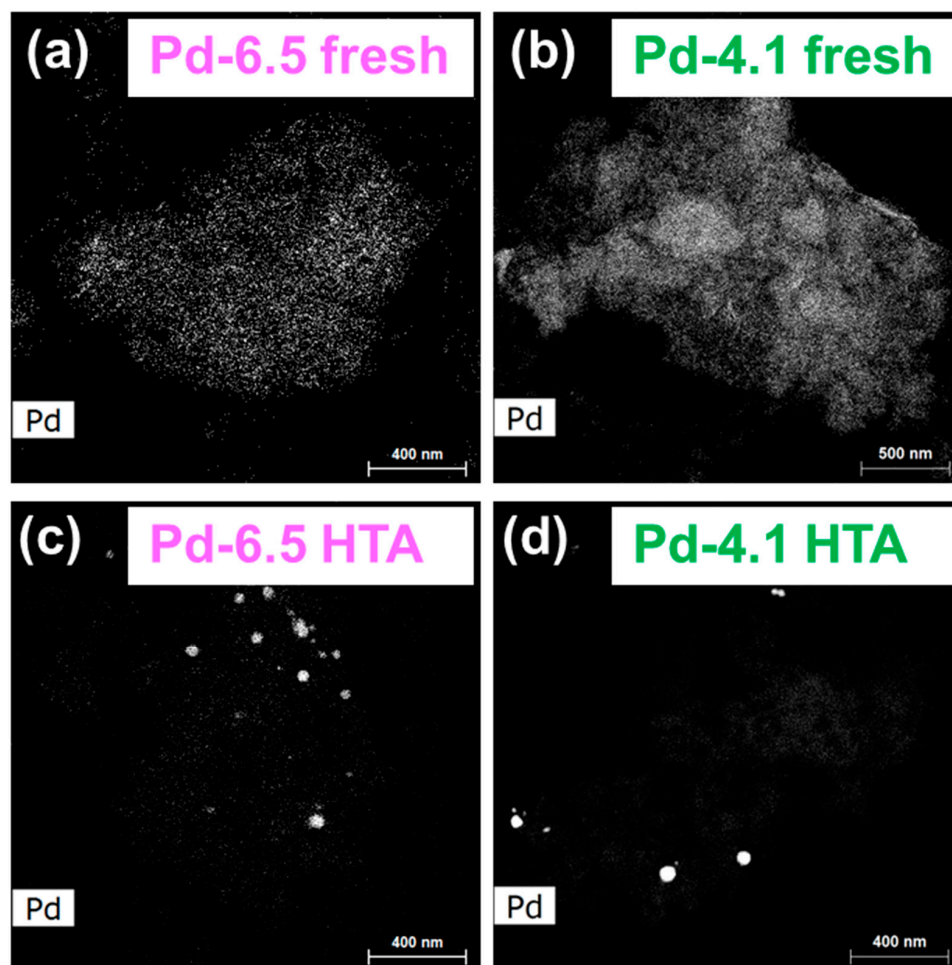


Figure 6. Oxygen storage capacity (OSC) for fresh Pd-6.5, Pd-4.1, and Pd-1.4, and HTA Pd-6.5 and Pd-4.1 samples.

Upon hydrothermal aging, both the Pd-6.5 and Pd-4.1 samples experienced a decline in their OSC performance, reflecting the detrimental impact of hydrothermal aging on the OSC material. Notably, even after aging, the Pd-6.5 sample continued to outperform the Pd-4.1 sample at both 350 °C and 550 °C. This suggests that while the larger pore volume of the Pd-4.1 sample offers advantages in its aged state, it might also pose challenges in retaining stability under hydrothermal conditions. The consistent superior performance of the Pd-6.5 sample underscores the pivotal role of Pd content in determining OSC efficiency, especially when subjected to aging.

### 3.3. Scanning Transmission Electron Microscopy (STEM) Analysis

Figure 7 provides insights into the dispersion and particle size of Pd in the catalyst samples through STEM imaging. In the fresh samples, as depicted in Figure 7a,b, Pd particles were well-dispersed and uniformly distributed across the sample, with their sizes consistently below 5 nm. On the other hand, following hydrothermal aging, as seen in Figure 7c,d, the Pd particles in the aged samples exhibited significant growth, with the STEM images revealing particle sizes exceeding 50 nm. This growth indicates significant agglomeration or sintering events during the aging process. Specifically, in the Pd-6.5 HTA sample, Pd particles were observed to range between 30 nm and 70 nm, whereas in the Pd-4.1 HTA sample, Pd particles below 50 nm were scarcely observed. Such a pronounced increase in particle size after aging not only highlights the substantial impact of hydrothermal conditions on the catalyst's structural changes but also suggests that these morphological alterations could adversely influence the catalyst's performance.



**Figure 7.** STEM images of Pd particles for fresh Pd-6.5 and Pd-4.1 TWC (a,b) and HTA (c,d) samples.

#### 4. Conclusions

This study's focal point was the evaluation of three-way catalysts (TWCs) with varying Pd loadings, particularly assessing their efficiency in propane reactivity for LPG engines. One of the most salient findings from this research was the performance exhibited by the fresh Pd-4.1 TWC sample with a high pore volume. Remarkably, even with its substantially reduced Pd content, this sample demonstrated performance comparable to or better than its Pd-6.5 counterpart in terms of NO and C<sub>3</sub>H<sub>8</sub> conversion efficiency and the water–gas shift (WGS) reaction. Furthermore, the oxygen storage capacity (OSC) results indicated that the fresh Pd-4.1 sample displayed higher OSC values than the Pd-6.5 sample at 550 °C, possibly due to its high pore volume. However, the challenges posed by hydrothermal aging became particularly evident when observing the more pronounced degradation in TWC performance for the Pd-4.1 sample compared to the Pd-6.5 sample, highlighting the critical importance of developing catalyst durability. Moreover, this study emphasizes the promising potential of eco-friendly fuels like LPG in curbing harmful emissions. However, the inherent slower reactivity of propane, its main component, underscores the need for developing catalysts that can efficiently address this challenge, especially during cold start conditions. Nevertheless, from an economic perspective, a Pd loading of 4.1 g/L is particularly attractive because the cost-efficiency of catalysts is a critical factor in their large-scale industrial application. Utilizing a reduced amount of Pd, as seen in the Pd-4.1 sample, without compromising on conversion efficiency, can lead to significant cost savings in catalyst production. However, it is important to note that real-world aging and thermal aging can impact a catalyst differently, potentially resulting in diverse conclusions. Additionally, the presence of elements like phosphorus (P) and zinc (Zn) in lubricants has been found to significantly affect the performance degradation of three-way catalysts. While this study primarily focuses on the performance of fresh samples with lower precious-metal content compared to those with higher Pd content, it suggests the need for further investigations into catalyst durability and catalyst poisoning. Therefore, while thermal aging offers valuable insights for accelerated testing and initial catalyst screening, considering real-world aging conditions is essential for a comprehensive understanding of catalyst performance and durability in practical applications. As the maritime industry navigates the complexities of emission regulations and the rising costs of precious metals, this study offers a beacon, guiding the way toward the development of efficient, durable, and economical emission control solutions.

**Funding:** This research received no external funding.

**Institutional Review Board Statement:** Not applicable.

**Informed Consent Statement:** Not applicable.

**Data Availability Statement:** The data used to support the findings of this study are included within the article.

**Acknowledgments:** I would like to express our gratitude to Nguyen Ke (UTK) and Todd J. Toops (ORNL) for their invaluable advice on the experiments and for granting permission to use the instruments. My appreciation also extends to Michael J. Lance (ORNL) for his expertise and assistance with the STEM analysis.

**Conflicts of Interest:** The authors declare no conflict of interest.

#### References

1. Ni, P.; Wang, X.; Li, H. A Review on Regulations, Current Status, Effects and Reduction Strategies of Emissions for Marine Diesel Engines. *Fuel* **2020**, *279*, 118477.
2. Smith, T.W.P.; Jalkanen, J.P.; Anderson, B.A.; Corbett, J.J.; Faber, J.; Hanayama, S.; O'Keeffe, E.; Parker, S.; Johansson, L.; Aldous, L.; et al. *Third IMO Greenhouse Gas Study 2014*; International Maritime Organization: London, UK, 2015.
3. DieselNet. IMO Marine Engine Regulations. Available online: <https://dieselnet.com/standards/inter/imo.php#other> (accessed on 24 October 2023).

4. Camarillo, M.K.; Stringfellow, W.T.; Hanlon, J.S.; Watson, K.A. Investigation of Selective Catalytic Reduction for Control of Nitrogen Oxides in Full-Scale Dairy Energy Production. *Appl. Energy* **2013**, *106*, 328–336. [CrossRef]
5. Ryu, Y.; Kim, H.; Cho, G.; Kim, H.; Nam, J. A Study on the Installation of SCR System for Generator Diesel Engine of Existing Ship. *J. Korean Soc. Mar. Eng.* **2015**, *39*, 412–417.
6. Raptotasiou, S.I.; Sakellariadis, N.F.; Papagiannakis, R.G.; Hountalas, D.T. Application of a Multi-Zone Combustion Model to Investigate the NO<sub>x</sub> Reduction Potential of Two-Stroke Marine Diesel Engines Using EGR. *Appl. Energy* **2015**, *157*, 814–823.
7. Verschaeren, R.; Schaepdryver, W.; Serruys, T.; Bastiaen, M.; Vervaeke, L.; Verhelst, S. Experimental Study of NO<sub>x</sub> Reduction on a Medium Speed Heavy Duty Diesel Engine by the Application of EGR (Exhaust Gas Recirculation) and Miller Timing. *Energy* **2014**, *76*, 614–621. [CrossRef]
8. Nam, J.-G. A Study of NO<sub>x</sub> Performance for Cu-Chabazite SCR Catalysts by Sulfur Poisoning and Desulfation. *J. Korean Soc. Mar. Eng.* **2013**, *37*, 855–861. [CrossRef]
9. Mukherjee, A.; Bruijninx, P.; Junginger, M. Techno-Economic Competitiveness of Renewable Fuel Alternatives in the Marine Sector. *Renew. Sustain. Energy Rev.* **2023**, *174*, 113127.
10. Kořwzan, K.; Narewski, M. Alternative Fuels for Marine Applications. *Latv. J. Chem.* **2012**, *51*, 398–406. [CrossRef]
11. Vandebroek, L.; Berghmans, J. Safety Aspects of the Use of LNG for Marine Propulsion. *Procedia Eng.* **2012**, *45*, 21–26. [CrossRef]
12. Beecken, J.; Mellqvist, J.; Salo, K.; Ekholm, J.; Jalkanen, J.-P. Airborne Emission Measurements of SO<sub>2</sub>, NO<sub>x</sub> and Particles from Individual Ships Using a Sniffer Technique. *Atmos. Meas. Tech.* **2014**, *7*, 1957–1968. [CrossRef]
13. Wattanavichien, K. Spray and Combustion Visualization of LPG-PME Dual Fuelling an IDI Compression Ignition Engine. In Proceedings of the 3rd Regional Conference on Mechanical and Aerospace Technology, Manila, Philippines, 24–25 March 2011; p. 15.
14. Arapatsakos, C.; Karkanis, A.; Katirtzoglou, G.; Pantokratoras, I. Liquid Petroleum Gas (LPG) and Natural Gas (NG) as Fuels on Diesel Engine–Dual Fuel Engine. In *Recent Advances in Fluid Mechanics and Heat & Mass Transfer, Proceedings of the 9th IASME/WSEAS International Conference on Fluid Mechanics & Aerodynamics (FMA '11) and the 9th IASME/WSEAS International Conference on Heat Transfer, Thermal Engineering and Environment (HTE '11), Florence, Italy, 23–25 August 2011*; WSEAS Press: Athens, Greece, 2011. Available online: <https://www.wseas.us/e-library/conferences/2013/Vouliagmeni/FLUHE> (accessed on 11 November 2023).
15. Gamas, E.D.; Diaz, L.; Rodriguez, R.; Lopez-Salinas, E.; Schifter, I.; Ontiveros, L. Exhaust Emissions from Gasoline-and LPG-Powered Vehicles Operating at the Altitude of Mexico City. *J. Air Waste Manag. Assoc.* **1999**, *49*, 1179–1189. [CrossRef]
16. Kim, K.; Kim, J.; Oh, S.; Kim, C.; Lee, Y. Lower Particulate Matter Emissions with a Stoichiometric LPG Direct Injection Engine. *Fuel* **2017**, *187*, 197–210. [CrossRef]
17. Werpy, M.R.; Burnham, A.; Bertram, K. *Propane Vehicles: Status, Challenges, and Opportunities*; Center for Transportation Research, Argonne National Laboratory: Argonne, IL, USA, 2010.
18. Chang, C.-C.; Lo, J.-G.; Wang, J.-L. Assessment of Reducing Ozone Forming Potential for Vehicles Using Liquefied Petroleum Gas as an Alternative Fuel. *Atmos. Environ.* **2001**, *35*, 6201–6211. [CrossRef]
19. Kang, S.B.; Nam, S.B.; Cho, B.K.; Nam, I.-S.; Kim, C.H.; Oh, S.H. Effect of Speciated HCs on the Performance of Modern Commercial TWCs. *Catal. Today* **2014**, *231*, 3–14. [CrossRef]
20. Emirođlu, A.O. Investigation of Effect of Propane and Methane Gases on Commercial Catalytic Converter Activity. *Int. J. Automot. Eng. Technol.* **2016**, *5*, 47–52. [CrossRef]
21. Di Maio, D.; Beatrice, C.; Guido, C.; Fraioli, V.; Napolitano, P.; Kannepalli, S.; Golini, S.; Tsinoglou, D. Methane Conversion and Ammonia Formation Model over a Pd-Rh Three-Way Catalyst for CNG Heavy-Duty Engines. *SAE Tech. Pap.* 2021. [CrossRef]
22. Di Maio, D.; Beatrice, C.; Fraioli, V.; Napolitano, P.; Golini, S.; Rutigliano, F.G. Modeling of Three-Way Catalyst Dynamics for a Compressed Natural Gas Engine during Lean–Rich Transitions. *Appl. Sci.* **2019**, *9*, 4610. [CrossRef]
23. Wang, M.; Eggenschwiler, P.D. Modeling of Three Way Catalyst Behavior Under Steady and Transient Operations in a Stoichiometric Natural Gas Fueled Engine. *SAE Tech. Pap.* **2021**. [CrossRef]
24. Twigg, M.V. Progress and Future Challenges in Controlling Automotive Exhaust Gas Emissions. *Appl. Catal. B* **2007**, *70*, 2–15. [CrossRef]
25. Kařpar, J.; Fornasiero, P.; Graziani, M. Use of CeO<sub>2</sub>-Based Oxides in the Three-Way Catalysis. *Catal. Today* **1999**, *50*, 285–298. [CrossRef]
26. Granger, P.; Lamonier, J.F.; Sargent, N.; Aboukais, A.; Leclercq, L.; Leclercq, G. Investigation of the Intrinsic Activity of Zr<sub>x</sub>Ce<sub>1-x</sub>O<sub>2</sub> Mixed Oxides in the CO+ NO Reactions: Influence of Pd Incorporation. *Top. Catal.* **2001**, *16*, 89–94. [CrossRef]
27. Heck, R.M.; Farrauto, R.J.; Gulati, S.T. *Catalytic Air Pollution Control: Commercial Technology*, 3rd ed.; John Wiley and Sons: Hoboken, NJ, USA, 2012; ISBN 9780470275030.
28. Yao, Y.F.Y.; Yu Yao, Y. The Oxidation of CO and Hydrocarbons over Noble Metal Catalysts. *J. Catal.* **1984**, *87*, 152–162. [CrossRef]
29. Cullis, C.F.; Willatt, B.M. Oxidation of Methane over Supported Precious Metal Catalysts. *J. Catal.* **1983**, *83*, 267–285. [CrossRef]
30. Rappé, K.G.; DiMaggio, C.; Pihl, J.A.; Theis, J.R.; Oh, S.H.; Fisher, G.B.; Parks, J.; Easterling, V.G.; Yang, M.; Stewart, M.L. Aftertreatment Protocols for Catalyst Characterization and Performance Evaluation: Low-Temperature Oxidation, Storage, Three-Way, and NH<sub>3</sub>-SCR Catalyst Test Protocols. *Emiss. Control Sci. Technol.* **2019**, *5*, 183–214. [CrossRef]

31. Li, P.; Chen, X.; Li, Y.; Schwank, J.W. A Review on Oxygen Storage Capacity of CeO<sub>2</sub>-Based Materials: Influence Factors, Measurement Techniques, and Applications in Reactions Related to Catalytic Automotive Emissions Control. *Catal. Today* **2019**, *327*, 90–115. [[CrossRef](#)]
32. Wang, J.; Chen, H.; Hu, Z.; Yao, M.; Li, Y. A Review on the Pd-Based Three-Way Catalyst. *Catal. Rev.* **2015**, *57*, 79–144. [[CrossRef](#)]
33. Han, Z.; Wang, J.; Yan, H.; Shen, M.; Wang, J.; Wang, W.; Yang, M. Performance of Dynamic Oxygen Storage Capacity, Water–Gas Shift and Steam Reforming Reactions over Pd-Only Three-Way Catalysts. *Catal. Today* **2010**, *158*, 481–489. [[CrossRef](#)]
34. Li, J.; Liu, X.; Zhan, W.; Guo, Y.; Guo, Y.; Lu, G. Preparation of High Oxygen Storage Capacity and Thermally Stable Ceria–Zirconia Solid Solution. *Catal. Sci. Technol.* **2016**, *6*, 897–907. [[CrossRef](#)]

**Disclaimer/Publisher’s Note:** The statements, opinions and data contained in all publications are solely those of the individual author(s) and contributor(s) and not of MDPI and/or the editor(s). MDPI and/or the editor(s) disclaim responsibility for any injury to people or property resulting from any ideas, methods, instructions or products referred to in the content.